ingegneria sismica
International Journal of Earthquake Engineering
Anno XLIII - Num. 3 - 2026

Node Frequency Spatiotemporal-Based Dynamic Partitioning and Online Regional Inertia Estimation Method for Power Systems

Zixuan Wang[1,*] *and Long Cheng*[1]

[1] School of Electrical Engineering, Northeast Electric Power University, Jilin, 132012, China

SUMMARY: *To address the strong time-varying characteristics and pronounced regional differences of power system inertia under high renewable energy penetration, this paper proposes an online regional inertia assessment method based on frequency dynamic partitioning. Real-time correlations among frequency trajectories are used to perform online frequency partitioning within a sliding time window via a Pearson-based spectral clustering approach. Dynamic Time Warping (DTW) and K-Medoids clustering are employed to select representative measurement points within each region, constructing equivalent regional frequency signals. Furthermore, the method integrates N4SID state-space identification with multiple inertia estimation techniques through statistical fusion to enhance robustness and accuracy. Simulation results on the modified IEEE 10-generator 39-bus system demonstrate that the proposed approach achieves high estimation accuracy and strong engineering applicability across different operating scenarios.*

KEYWORDS: *Regional Inertia Estimation; Frequency Response; Dynamic Partitioning; N4SID*

1 Introduction

In recent years, power systems have been rapidly evolving toward a “dual-high” paradigm characterized by high penetration of renewable energy sources and extensive integration of power electronic devices. The large-scale grid integration of renewable energy has significantly altered the inertia composition of the system. In particular, the continuous reduction in the share of conventional synchronous generators has led to a persistent decline in the overall equivalent rotational inertia, making inertia degradation an increasingly prominent issue [1]. With the growing penetration of renewables, insufficient system inertia has exerted a significant impact on secure and stable grid operation [2, 3]. In dual-high power systems, the scale of renewable integration, operating conditions, and control strategies exhibit pronounced temporal variability and spatial distribution characteristics. Consequently, system inertia levels demonstrate substantial variations across different time instants and geographical regions [4]. Especially following disturbances, the frequency response trajectories and inertia support capabilities of different regions are markedly unbalanced. Under such circumstances, a single system-wide equivalent inertia index is no longer sufficient to accurately characterize local frequency dynamics or to reflect their influence on overall system stability, thereby constraining the system’s renewable energy accommodation capability [5]. Moreover, renewable energy units such as wind turbines can participate in frequency support through virtual inertia control. However, their inertial response differs fundamentally from the physical rotational inertia of

*13633551695@163.com
https://doi.org/10.65102/is20261262 Published: 10 June, 2026

conventional synchronous machines in terms of magnitude, duration, and activation conditions. This further enhances the dynamic variability and uncertainty of regional inertia characteristics. Therefore, accurate assessment of regional and system-wide inertia levels under varying renewable penetration scenarios is of significant theoretical importance and practical engineering value for ensuring frequency stability in dual-high power systems.

At the current stage of power system operation, Phasor Measurement Unit (PMU)–based monitoring devices and Wide Area Measurement System (WAMS) have been widely deployed [6], providing abundant real-time measurement data with high temporal resolution to support online inertia estimation. In studies on inertia online assessment based on PMU data, if a single synchronous generator or its point of interconnection (POI) is taken as the minimum evaluation unit, the computational burden becomes substantial, and it is difficult to meet the requirements of real-time online applications [7]. To address the issue that estimation accuracy is constrained by uncertainty in model order during system identification–based online inertia evaluation, Reference [8] employed the Akaike Information Criterion (AIC) to adaptively determine the optimal model order. Based on the response of the identified model, online inertia estimation was then performed, and simulation results verified the accuracy and effectiveness of the proposed approach. However, when the entire power system is considered as the evaluation scope, it is generally necessary to obtain the total system power imbalance in advance. Such methods are typically applicable only to inertia estimation following large disturbances, such as generator tripping or DC blocking events [9–11], and therefore are not suitable for continuous online monitoring of system inertia levels under normal operating conditions.

Considering that the frequency dynamic response of power systems exhibits pronounced spatial heterogeneity [12], and that variations in active power flows across tie-lines can effectively reflect the degree of power imbalance among different areas, conducting online inertia assessment at the regional level offers greater engineering feasibility and operational flexibility. Reference [13] proposed a method for estimating the total system inertia based on PMU-measured transient frequency data. In this approach, event detection and signal filtering techniques are employed to extract regional inertia, which is subsequently aggregated to obtain the overall system inertia. In addition, the residual inertia contributions from loads and distributed energy resources are evaluated. Based on the above research framework, the related literature can be systematically reviewed from two key perspectives: regional partitioning methods for power system frequency dynamic responses, and inertia parameter identification techniques.

In studies on regional partitioning of power system frequency dynamic responses, Reference [14] proposed a near-continuous online estimation method for the equivalent inertia of the entire power system and its subregions based on PMU ambient measurements and system identification techniques. Reference [15] revealed that neither at the same location nor across different regions can a single control strategy simultaneously and optimally improve all frequency performance indices. Instead, frequency support schemes should be purposefully configured according to the specific frequency issues of concern. Regions characterized by low inertia and located far from the center of inertia (COI) are more sensitive in terms of frequency and oscillatory dynamics; therefore, they should be classified as independent frequency response zones and prioritized for frequency support allocation [16]. However, the above model-based partitioning approaches generally result in static and fixed regional division schemes, which are difficult to adapt to varying operating conditions and diverse disturbance scenarios. To address this limitation, Reference [17] proposed a power system partitioning method that integrates modal frequency decomposition, quantitative analysis of frequency response characteristics, and an improved k-means clustering algorithm. Reference [18] employed algebraic graph theory to decompose globally coupled voltage–frequency dynamic

responses into several locally coupled components, thereby achieving dynamic system partitioning. Nevertheless, these dynamic approaches are primarily applicable to small-disturbance or linearized dynamic analyses and are therefore insufficient to meet practical requirements under varying operating conditions and large-disturbance scenarios.

In the field of power system parameter identification, extensive efforts have been devoted to exploring inertia estimation methods from various perspectives. Reference [19] proposed a method for estimating regional and system-wide total inertia based on transient frequency measurements obtained from PMUs. Reference [20] introduced a prediction error minimization (PEM)–based SSEST model, providing an optimal fitting framework for online measurement of equivalent system inertia and enabling fast and accurate inertia estimation. Reference [21] investigated unified modeling approaches for grid-connected equipment clusters, as well as principles and methodologies for inertia response matching. Reference [22] constructed an association model between rotor speed and bus frequency by exploiting the spatial correlation of system frequency and properly configured PMU data, thereby enabling real-time online inertia estimation and monitoring of inertia distribution. Reference [23] proposed a data-driven method based on frequency gradients to estimate time-varying system inertia from a reduced-order dynamic model under normal operating conditions; however, this approach is only applicable to offline inertia estimation. Reference [24] employed a Box–Jenkins identification model, with the Akaike Information Criterion (AIC) used to determine the optimal model order, to perform regional inertia parameter identification. Nevertheless, as a black-box modeling approach, this method cannot explicitly represent system states, resulting in limited model interpretability. Therefore, it is necessary to develop a system identification model capable of explicitly describing the input–output relationship, so as to clearly characterize the mathematical process underlying inertia estimation.

In summary, existing research on online inertia assessment in power systems still exhibits several notable limitations: 1) Insufficient adaptability of regional partitioning methods to time-varying conditions. Most regional partitioning approaches are still based on static division schemes. Even when dynamic partitioning mechanisms are introduced, the analysis is typically conducted under small-disturbance or linearized assumptions. As a result, these methods are unable to adequately capture the time-varying evolution characteristics of frequency dynamic responses under large disturbances and complex operating condition changes, thereby limiting their applicability in practical operation scenarios. 2) Limited robustness in the construction of regional equivalent frequency. Many existing regional inertia estimation methods implicitly assume that frequency responses of measurement points within the same region remain temporally synchronized. However, in practical power systems, measurement delays, communication latencies, and differences in local control strategies are commonly present among different nodes. Under such conditions, directly using the arithmetic average frequency or the center-of-inertia (COI) frequency as the regional equivalent frequency may amplify measurement noise and timing deviations, which in turn degrades the stability and accuracy of inertia estimation results. 3) Single identification methodology and limited model interpretability. Current inertia estimation studies often rely on a single identification approach, such as methods based on the initial rate of change of frequency (RoCoF), polynomial fitting techniques, integral-based methods, or Box–Jenkins (BJ) models. A single method generally struggles to maintain stable estimation accuracy under different disturbance types and operating conditions. Moreover, certain black-box models fail to explicitly describe the physical relationships among system inputs, states, and outputs, thereby constraining the interpretability of inertia estimation results and their practical engineering value.

To address the above issues, this paper proposes an online regional inertia assessment method for power systems oriented toward frequency dynamic responses, and establishes a

unified analytical framework of “dynamic partitioning – representative node selection – multi-method fusion estimation.” The proposed method performs online analysis of measured frequency trajectories following different disturbance events, enabling dynamic partitioning and adaptive updating of system regions. In this way, the rationality of the partitioning results under complex operating conditions can be effectively reflected. Subsequently, representative nodes within each region are accurately selected to construct reliable regional equivalent frequency signals. Finally, a multi-method fusion strategy is employed to enhance the accuracy and robustness of regional inertia estimation. The overall procedure of this study is summarized as follows:

First, starting from the fundamental mechanism of power system frequency dynamic responses, the basic principles of online regional inertia assessment are systematically elaborated. Subsequently, a similarity matrix among measurement nodes is constructed based on the correlation characteristics of real-time frequency trajectories. Within a sliding time window, a spectral clustering (SC) method based on the Pearson correlation coefficient is employed to characterize the synchronization of frequency responses among measurement nodes, thereby enabling online correction and time-varying updating of frequency dynamic partitions.

On this basis, to address potential time delays and local temporal stretching effects in frequency responses within the same region, the Dynamic Time Warping (DTW) distance is introduced to quantify the similarity between frequency curves. Combined with the K-medoids clustering algorithm, the most representative frequency measurement node in each region is selected to construct the regional equivalent frequency signal, which serves as the input for regional frequency dynamic modeling.

Subsequently, the Numerical algorithms for Subspace State Space System Identification (N4SID) method is adopted to model the regional power–frequency dynamic process. In combination with multiple inertia estimation techniques—including the Rate of Change of Frequency (RoCoF) method, weighted least squares (WLS), and the integral method—regional inertia parameters are comprehensively estimated. By statistically fusing the results obtained from different estimation methods, the sensitivity of any single method to noise and modeling errors is effectively suppressed, leading to more robust and accurate regional inertia assessment outcomes.

Finally, the modified IEEE 10-generator 39-bus system is employed as a case study to systematically validate the proposed dynamic partitioning method and regional inertia estimation strategy in terms of estimation accuracy, real-time updating capability of partitioning results, and adaptability under different operating scenarios. Simulation results demonstrate that the proposed approach exhibits strong effectiveness and promising engineering application value.

2 Regional Inertia Estimation Principle of Power Systems

This section first introduces the conventional regional inertia estimation methods for traditional power systems, along with their underlying modeling principles. On this basis, a regional inertia assessment approach for power systems with renewable energy integration is subsequently developed. Furthermore, the applicability and analytical scope of the proposed model under different disturbance scenarios are systematically clarified.

2.1 Modeling and Analysis of Regional Inertia in Conventional Power Systems

In conventional power systems, when a power imbalance disturbance occurs, the system frequency response can be divided—according to time scale and the physical mechanisms involved in regulation—into three successive stages: instantaneous disturbance power allocation, inertial response, and primary frequency control. The detailed frequency response process is illustrated in Figure 1. At the instant of disturbance, the disturbance power is instantaneously distributed among synchronous generators according to the synchronizing power coefficients between the disturbance location and each generator (which are inversely proportional to the electrical distance). During this stage, inertia does not participate in the response, and the system frequency remains unchanged. Subsequently, the system enters the inertial response stage. Within the first few seconds after the disturbance, primary frequency control remains inactive because the frequency deviation is within the governor deadband (0–0.033 Hz). Hence, the disturbance power is shared among generating units according to their inertia time constants, resulting in a decrease or increase in system frequency.

When the frequency deviation exceeds 0.033 Hz, primary frequency control becomes activated and begins to regulate the system frequency. After the governor action is completed, the system reaches a new steady state, in which the disturbance power is allocated according to the governor gain (i.e., the reciprocal of the droop coefficient), thereby achieving active frequency regulation.

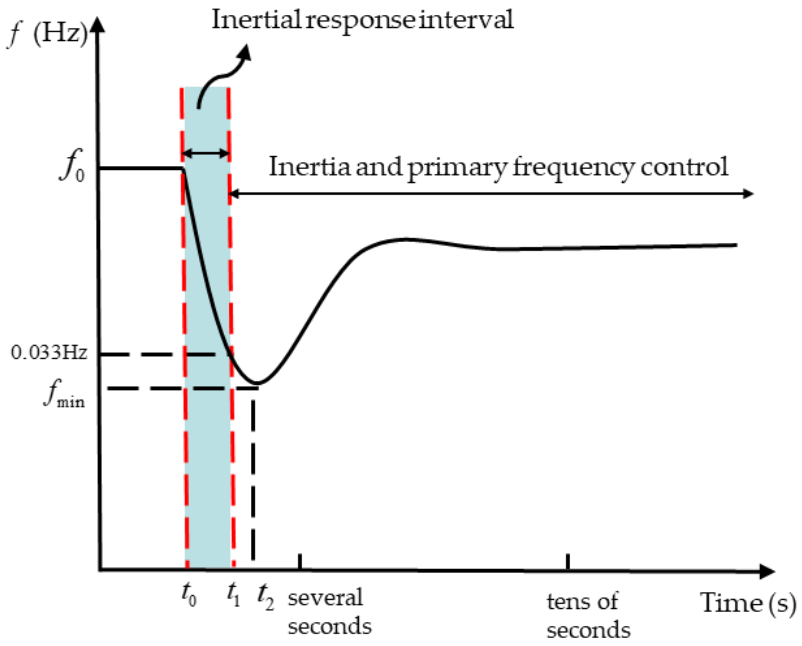

Figure 1: Time sequence diagram of systemfrequency response

The rotor motion equation of synchronous generators in a conventional power system region can be expressed as:

$$2H_m \frac{df_m}{dt} + D_m \Delta f_m = \Delta P_m^j - \Delta P_e^j - \Delta P_L^k - \Delta P_l^h \quad (1)$$

$$\begin{cases} \Delta P_m = \Delta P_m^j - \Delta P_e^j - \Delta P_L^k - \Delta P_l^h - D_m \Delta f_m \\ J_m = \dfrac{df_m}{dt} \\ H_m = -\dfrac{\Delta P_m}{2J_m} \end{cases} \tag{2}$$

where H_m is the inertia time constant of conventional generators in the region; f_m denotes the frequency of the regional synchronous generators; D_m represents the damping coefficient of the regional synchronous generators; Δf_m is the frequency deviation of the regional synchronous generators; ΔP_m^j is the variation in mechanical power of the j-th synchronous generator in the region; ΔP_e^j is the variation in electromagnetic power of the j-th synchronous generator; ΔP_L^k is the active power variation of the *k*-th load in the region; ΔP_l^h is the active power variation of the h-th tie-line in the region; J_m denotes the frequency variation of the equivalent regional synchronous generator; and ΔP_m represents the total power variation of the equivalent regional synchronous generator.

2.2 Regional Inertia Modeling and Analysis of Power Systems with Renewable Energy Integration

With the large-scale grid integration of renewable energy generation units, inertia support in power systems is no longer provided solely by synchronous generators. Un-der the maximum power point tracking (MPPT) operating mode, doubly fed induction generator (DFIG)–based wind turbines can participate in system frequency regulation by incorporating a composite inertia control loop, thereby delivering a virtual inertia response that is significantly larger than that corresponding to the turbine's inherent mechanical inertia time constant when a disturbance occurs.

This composite inertia control strategy consists of two components: virtual inertia control and droop control. The control structure is illustrated in Figure. 2. In this framework, ω denotes the turbine rotor speed, f_n is the rated system frequency, f_w represents the frequency at the wind turbine terminal, P_w is the total active power output of the wind turbine, P_{MPPT} is the reference active power under MPPT operation, ΔP_1 and ΔP_2 denote the active power variations induced by the droop control and virtual inertia control loops, respectively, and K_1 and K_2 are the virtual inertia control gain and the droop control gain, respectively.

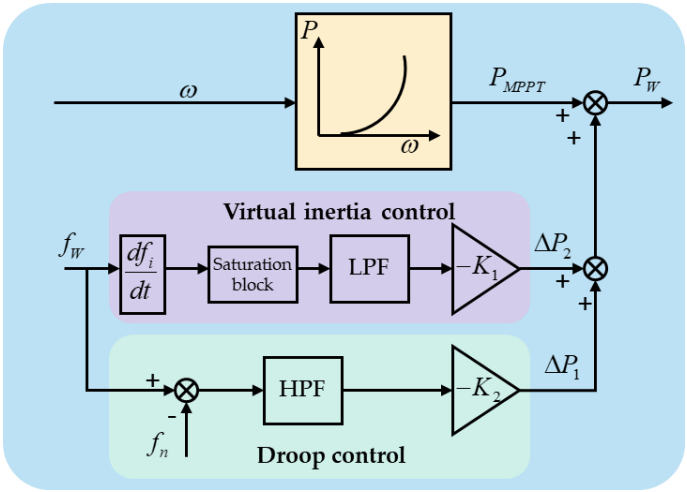

Figure 2: Block diagram of integrated inertia control

When the wind turbine participates in frequency regulation, its active power output can be expressed as:

$$P_w = P_{MPPT} - K_1 \frac{df_i}{dt} - K_2 \Delta f_i \tag{3}$$

where f_i denotes the frequency of the equivalent regional generator, and Δf_i represents the regional frequency deviation under the disturbance.

During the regional inertia response process of a power system, the inertia component is the first to take effect in frequency dynamics. After virtual inertia control and droop control are introduced for doubly fed wind turbines, the installed capacities of all synchronous generators within the region are first aggregated into an equivalent synchronous generator. Subsequently, an equivalent regional generator model is established based on the rotor motion equation. At the instant when the synchronous generator is subjected to a disturbance, the variation characteristics of regional active power are illustrated in Figure 3. Following the treatment in (1), the relevant control parameters in (3) are incorporated into the rotor motion equation, from which (4)–(6) can be further derived.

$$\begin{cases} 2H_d = 2\left(H_i + \dfrac{K_1}{2S_N}\right) \\ D_d = D_i + \dfrac{K_2}{2S_N} \end{cases} \tag{4}$$

$$2H_d \frac{df_i}{dt} + D_d \Delta f_i = \Delta P_w + \Delta P_m - \Delta P_e - \Delta P_L^k - \Delta P_L^h \tag{5}$$

$$\begin{cases} \Delta P_d = \Delta P_w + \Delta P_m - \Delta P_e - \Delta P_L^k - \Delta P_L^h \\ J_i = \dfrac{df_i}{dt} \\ H_d = -\dfrac{\Delta P_d}{2J_i} \end{cases} \tag{6}$$

where S_N denotes the rated capacity of conventional generators in the region; H_d is the regional inertia time constant; D_i represents the equivalent damping coefficient of the regional generators; J_i is the rate of change of the equivalent regional generator frequency; and ΔP_d denotes the regional active power variation.

Based on the regional inertia time constants obtained from (4), the system-level inertia time constant can be further derived, with its mathematical expression given in (7).

$$H_x = \frac{\sum_{i=1}^{n} H_{di} S_i}{\sum_{i=1}^{n} S_i} \tag{7}$$

where H_{di} is the inertia time constant of region i, S_i denotes the rated capacity of the equivalent generator in region i, and n is the total number of system regions.

2.3 Regional Inertia Estimation Methods under Different Disturbance Scenarios

In practical power system operation, the system may experience both sudden large disturbances and continuous random small perturbations. Under small-disturbance conditions, frequency deviations typically remain within the primary frequency control (PFC) deadband, so the governors do not respond, and the system primarily relies on inertia and damping to suppress frequency variations. When a large disturbance occurs, frequency deviations exceed the deadband, and the governors participate in the regional primary frequency control process, acting together with the inertia response. Therefore, when performing regional inertia estimation, it is necessary to analyze the applicability of inertia identification models under different disturbance conditions. Based on this consideration, the transfer function model of regional inertia can be constructed with the active power disturbance ΔP_d as the input and the frequency deviation ΔJ_i as the output.

During normal power system operation, small random disturbances are always present. Since the primary frequency control does not act in this case, it can be assumed that $\Delta P_m = 0$. Under this condition, applying the Laplace transform to (5) yields the corresponding transfer function, as expressed in (8).

$$G_1(s) = \frac{\Delta J_i(s)}{\Delta P_d(s)} = -\frac{1}{2H_d s + D_d} \tag{8}$$

By applying the inverse Laplace transform to (8), the corresponding time-domain expression can be derived, with the specific result given in (9).

$$g_1(t) = -\frac{1}{2H_d} e^{-\frac{D_d}{2H_d}t} \tag{9}$$

where $g_1(t)$ represents the time-domain expression of the inertia response component. At t=0, $g_1(0) = -1/(2H_d)$. It can thus be seen that the equivalent regional inertia is numerically equal to the negative reciprocal of twice the inertia parameter. For large-disturbance scenarios, Ref. [16] indicates that the dynamic behavior of inertia during the initial stage of a disturbance can

be regarded as the initial impulse response obtained from the Laplace transform of the corresponding transfer function. Under such large-disturbance conditions, the associated transfer function is expressed as in (10).

$$G_2(s)=\frac{\Delta J_i(s)}{\Delta P_d(s)}=-\frac{1}{2H_d s+D_d+G_3(s)} \tag{10}$$

$$G_3(s)=\frac{1}{(Ts+1)R} \tag{11}$$

where $G_3(s)$ is the transfer function of the primary frequency control, T is the high-pressure steam volume time constant, and R is the droop control gain. According to the initial value theorem, as t=0 and $s \to \infty$, we obtain:

$$sG_2(s)\big|_{s=\infty}=-\frac{1}{2H_d s+D_d+G_3(s)}\Big|_{s=\infty}=-\frac{1}{2H_d} \tag{12}$$

From (9) and (12), it can be seen that, regardless of whether the system operates under small-disturbance or large-disturbance conditions, the established transfer function model can effectively provide estimates of the regional inertia time constant.

3 Real-Time Partitioning and Regional Frequency Dynamic Node Selec-tion Considering Power System Frequency Dynamic Responses

This section first proposes a quantitative index based on nodal frequency similarity and employs real-time frequency measurements obtained from PMUs to partition the system into coherent regions. On this basis, the node that provides the best regional frequency fitting is identified for each region.Furthermore, by analyzing the correlation of the frequency trajectories of these best-fit nodes, the set of nodes exhibiting coherent frequency dynamic responses during the disturbance is identified. This enables online correction and dynamic updating of the frequency dynamic partitioning, thereby capturing the time-varying characteristics of regional coherency throughout the disturbance process.

3.1 Frequency Dynamic Partition Updating Based on Pearson-Correlation-Based Spectral Clustering

Power system regional partitioning has traditionally relied on geographical proximity and operational experience. However, with the increasing structural com-plexity of modern power grids, such conventional partitioning methods often fail to satisfy the higher requirements of consistency with the system's internal dynamic electrical characteristics. To enable real-time partitioning of frequency dynamic re-sponses, it is first necessary to construct a quantitative metric that captures the simi-larity of node frequency behaviors. Although electrical distance is commonly used to characterize the strength of coupling between nodes, it cannot directly reflect fre-quency dynamic characteristics, nor can it capture the differences in system partition-ing features under varying disturbance conditions. Consequently, electrical distance is not suitable as a metric for node frequency similarity. To ensure that the partitioning results directly represent frequency dynamic responses while accounting for time-varying disturbances and

operating points, this paper adopts a Pear-son-correlation-based spectral clustering approach. Specifically, the consistency of frequency variation trends among nodes at the onset of a disturbance is analyzed to construct a similarity matrix, which is then used as the input to spectral clustering to achieve dynamic system partitioning.

The Pearson correlation coefficient is a statistical measure widely used in time-series analysis to quantify the degree of linear correlation between two random variables. Let $x=[x_1,x_2,\ldots,x_n]$ 和 $y=[y_1,y_2,\ldots,y_n]$,denote two measurement sequences within a given time window; the Pearson correlation coefficient between them is defined as:

$$p=\frac{\sum_{i=1}^{n}(x_k-\bar{x})(y_k-\bar{y})}{\sqrt{\sum_{i=1}^{n}(x_k-\bar{x})^2}\sqrt{\sum_{i=1}^{n}(y_k-\bar{y})^2}} \tag{13}$$

In the formula, x_k and y_k represent the *i*-th observation from populations x and y, respectively; $\bar{x}$ and $\bar{y}$ denote the means of sequences x and y within the time window. The coefficient ranges from [0,1], and a larger absolute value indicates a stronger linear correlation between the two sequences. When the correlation coefficient approaches 1, it signifies a high consistency in the variation trends of the two sequences.

In the dynamic frequency analysis of power systems, the frequency responses at different nodes under disturbances typically exhibit trends of synchronous acceleration or deceleration. The Pearson correlation coefficient is effective in characterizing the consistency of frequency variation trends among different nodes when subjected to disturbances. Moreover, this method is insensitive to variations in the amplitude of frequency, making it suitable for measuring the similarity of frequency dynamics across nodes of different capacities and electrical locations. Additionally, this index is calculated directly based on measured data, eliminating the need for reliance on system topology or precise parameter models, thus demonstrating strong applicability in engineering practice.

Based on the aforementioned characteristics, this paper conducts pairwise correlation analysis on real-time frequency trajectories from PMU measurement points within a sliding time window, employing the Pearson correlation coefficient. A frequency dynamic similarity matrix between nodes is constructed to reflect the synchronization relationships of frequency responses among nodes under the current operating state of the system. This similarity matrix is then used as the input for the subsequent spectral clustering (SC) algorithm, thereby enabling frequency-based dynamic partitioning of the power system.

Compared to traditional clustering methods based on distance or local criteria, Spectral Clustering (SC) avoids falling into local optima and is better suited for systems with significant global coupling characteristics. As a modern clustering algorithm grounded in graph theory, SC transforms the clustering problem into a graph partitioning problem. Unlike traditional clustering algorithms, SC employs distinct Laplacian matrices and indicator vectors, enabling the effective partitioning of data with varying distributions. This approach offers greater adaptability and stability.

The fundamental workflow of the algorithm is outlined as follows:

1) Consider an undirected weighted graph $G=(V,E)$, where $V=\{v_1,v_2,v_3,\ldots,v_n\}$ is the set of nodes sampled from the data; *E* is the set of edges, which defines the similarity between samples. The weight of the edge between nodes v_i and v_j is denoted as w_{ij} , and the weights for all nodes can be represented by the adjacency matrix W . Accordingly, the degree of a node can be defined by the formula:

$$d_i = \sum_{j=1}^{10} w_{ij} \tag{14}$$

In this paper, the frequency dynamic correlation between generators is used as the similarity measure to construct the adjacency matrix of the generator dynamic coupling graph, which characterizes the dynamic synchronous coupling strength between generator nodes. The Pearson correlation coefficient matrix is employed as the adjacency matrix W, and the corresponding formula for the number of partitions m is as follows:

$$W = \begin{bmatrix} |p_{11}| & |p_{12}| & \cdots & |p_{1N}| \\ |p_{21}| & |p_{22}| & \cdots & |p_{2N}| \\ \vdots & \vdots & \ddots & \vdots \\ |p_{N1}| & |p_{N2}| & \cdots & |p_{NN}| \end{bmatrix} \tag{15}$$

From Equation (14), the degree matrix D for all points can be obtained, where D is a diagonal matrix. The adjacency matrix, which describes the similarity between sample points, is commonly constructed using methods such as the ε-neighborhood method, the K-nearest neighbors method, or the fully connected method.

2) Calculate the normalized Laplacian matrix L_{N}.

If there exists a random vector f, and L is a real symmetric and positive semidefinite matrix whose eigenvalues are all nonnegative, then the following relation holds:

$$f^T L f = \frac{1}{2} \sum_{i=1}^{n} \sum_{j=1}^{n} w_{ij} \left(f_i - f_j \right)^2 \tag{16}$$

The normalized Laplacian matrix L_{N} and the random-walk Laplacian matrix L_{rw} are among the most commonly used forms of normalized Laplacian matrices. Their specific expressions are given as follows:

$$L_N = I - D^{-1/2} W D^{1/2} \tag{17}$$

$$L_{rw} = I - D^{-1} W \tag{18}$$

3) The eigenvectors corresponding to the first k eigenvalues of L are computed and assembled to form the feature matrix $H_{n \times k}$.

4) Based on $u_{ij} = h_{ij} / \sqrt{\sum_k h_{ik}^2}$, the matrix **H** is obtained by performing row-wise normalization.

5) The sample feature vectors are then clustered, i.e., graph partitioning is performed. Commonly used graph cut criteria include the minimum cut, average cut, and normalized cut. Let A and B denote two disjoint subsets; the cut between A and B can be expressed as:

$$cut(A, B) = \sum_{i \in A,\, j \in B} \omega_{ij} \tag{19}$$

6) The output is the partition of samples into subsets $A_1, A_2, \ldots, A_k$.

To further characterize the morphological similarity of nodal frequency response trajectories, a curve clustering algorithm based on the Fréchet distance is employed in the spectral embedding space to group the samples. Unlike the conventional Euclidean K-means

clustering method, Fréchet-based curve clustering comprehensively accounts for both the overall variation trend and the temporal continuity of frequency response trajectories, thereby enabling accurate partitioning of nodes with similar inertial dynamic characteristics. The output of this procedure assigns each node to a specific dynamic inertia region. Finally, the clustering results are evaluated by introducing the mean and median values of the intra-regional correlation coefficients. Larger values of these two indices indicate higher internal consistency within clusters and more pronounced inter-cluster separation.

In summary, this paper enhances the conventional spectral clustering framework by incorporating the Pearson correlation coefficient, an adaptive eigenvector selection mechanism, and Fréchet-distance-based curve clustering. Based on these improvements, a regional partitioning method tailored to the frequency dynamic response characteristics of power systems is established.

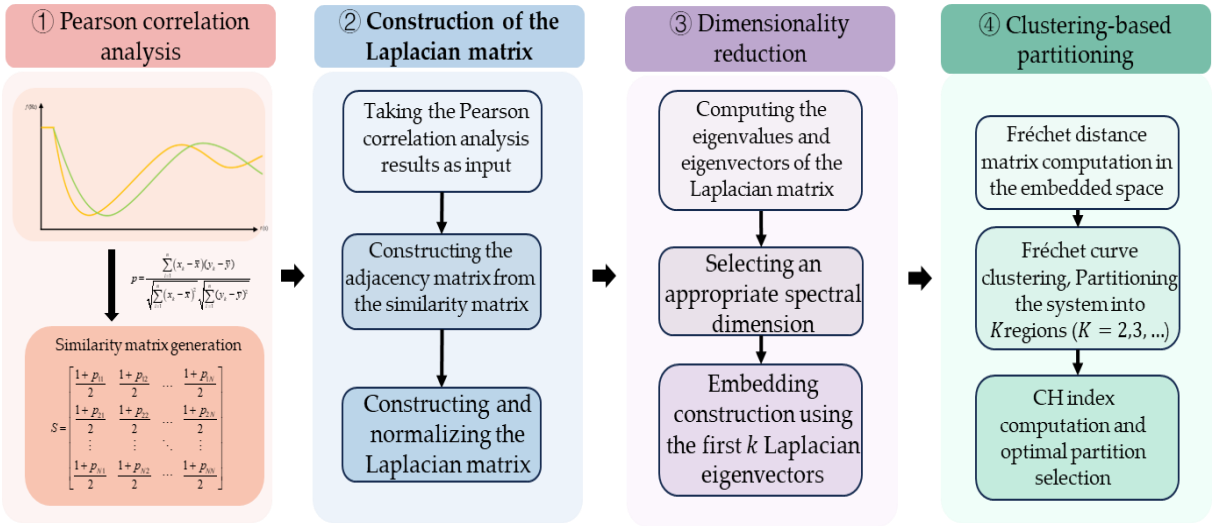

Figure 3: Flow chart of system partition

3.2 Regional Dynamic Node Selection Considering Node Frequency Similarity

The conventional approach of using the regional center-of-inertia (COI) frequency as the representative measurement for a region essentially computes a weighted aver-age of the node frequencies within the region. This method is limited in its ability to accurately capture the spatial distribution characteristics of frequency dynamic re-sponses, and its effectiveness in representing equivalent regional inertia further di-minishes under high renewable energy penetration. Therefore, it is necessary to recon-sider the selection of nodes that can faithfully represent the regional frequency varia-tion trends. Figure 4 illustrates the frequency response curves of two adjacent nodes in the system, which should be assigned to the same region. The similarity between node fre-quencies can be characterized from two perspectives. First, from a numerical stand-point, the frequency response curves are very close in value at any given time instant. Second, from a morphological perspective, the trajectories exhibit similar patterns, in-cluding short-term lead or lag characteristics. This behavior arises because, in a large power grid, disturbance propagation occurs as a wave process, and the timing with which different nodes experience the disturbance is closely related to their electrical distance from the disturbance source. Therefore, a metric for node frequency similarity should account for both the numerical differences in frequency responses and their lead-lag features.

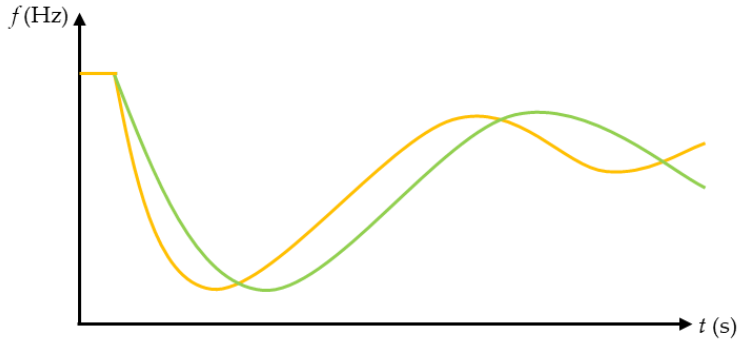

Figure 4: Dynamic schematic diagram of node frequency

The Dynamic Time Warping (DTW) algorithm is a method for measuring the similarity between two time series, particularly suitable for comparing sequences that are not aligned along the time axis. Based on this characteristic, DTW can serve as a metric for node frequency similarity. Let the PMU master station collect the discrete frequency sequences of two nodes as f^1 and f^2, each with a sequence length of r. Both sequences are of length:

$$f^1 = \left\{ f_1^1, f_2^1, \ldots, f_m^1, \ldots, f_r^1 \right\} \tag{20}$$

$$f^2 = \left\{ f_1^2, f_2^2, \ldots, f_n^2, \ldots, f_r^2 \right\} \tag{21}$$

Figure 5 illustrates the $r \times r$ grid matrix used for DTW path analysis, where the horizontal and vertical axes correspond to the frequency sequences f^1 and f^2, respectively. Each matrix element is denoted as $z_k(m,n)$, representing the association between the m-th sample point of f^1 and the n-th sample point of f^2. The DTW path extends from the starting point of the frequency sequences to the ending point and can be expressed as $Z = \{z_1, z_2, \ldots, z_s, \ldots, z_u\}$ where the path length satisfies $r \le u \le 2r$, and continuity and monotonicity constraints must be maintained along the path.

For continuity, any two consecutive points on the path, denoted as $z_k(m,n)$ and $z_{k+1}(m',n')$, must satisfy $(m'-m) \le 1$ and $(n'-n) \le 1$. This ensures that every sample point of the frequency sequences x and y is included in the computation, while the time warping accounts for lead-lag characteristics in the frequency trajectories.

In terms of monotonicity, for two consecutive points z_k and z_{k+1}, it is required that $m \le m'$ and $n \le n'$, so as to ensure that the correspondence between sampling points in the two sequences is counted only once and no sample pairing is repeatedly included.

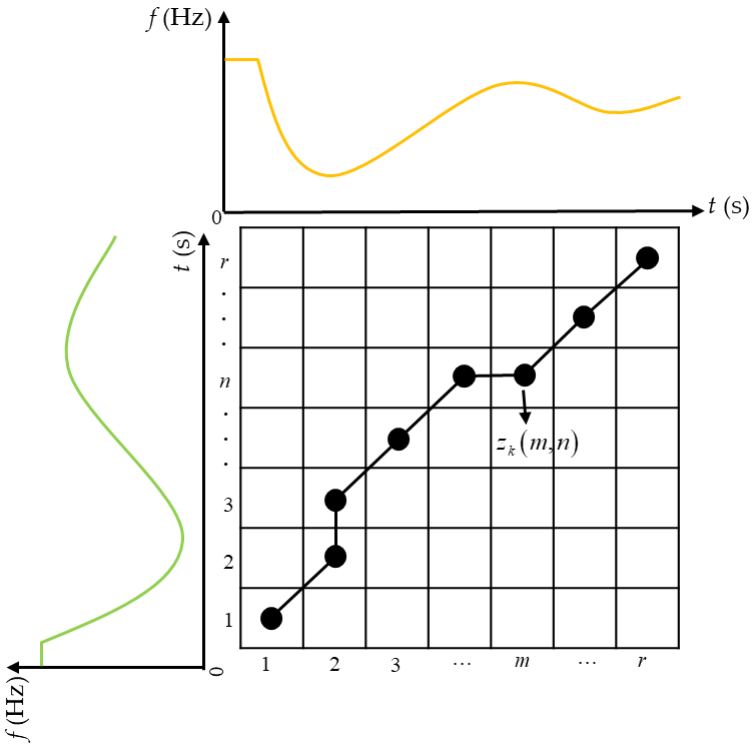

Figure 5: DTW path example diagram

The frequency deviation between the two sampling points f_m^1 and f_n^2 associated with element $z_k(m,n)$ is defined as $l(z_k)=l(m,n)=\left|f_m^1-f_n^2\right|$. For an arbitrary warping path, the cumulative frequency deviation is obtained by summing the deviations of all elements along the path. The path that yields the minimum cumulative deviation is regarded as the optimal alignment path, and the corresponding minimum cumulative value is defined as the DTW distance L_{DTW} between sequences f_m^1 and f_n^2.

$$L_{DTW}\left(f_m^1, f_n^2\right)=min\sum_{k=1}^{u} l(z_k) \tag{22}$$

The optimal path determination described in (22) is essentially a global optimization problem. By adopting the dynamic programming strategy formulated in (23), the global optimization process can be decomposed into a sequence of recursively solved local optimal decisions, thereby ensuring the attainment of the global optimal solution.

$$L(m,n)=l(m,n)+min\begin{cases} l(m,n-1) \\ l(m-1,n-1) \\ l(m-1,n) \end{cases} \tag{23}$$

where $L(m,n)$ denotes the minimum accumulated frequency deviation. Based on this definition, a node frequency similarity metric is constructed.

When the DTW distance between nodes is small, it indicates a high degree of consistency in their frequency variation characteristics, and such nodes can therefore be grouped into the same region. Accordingly, the online partitioning of frequency dynamic responses can be

realized on the basis of the DTW distance metric in conjunction with clustering techniques. Typical distance-based clustering algorithms include *k*-means and *k*-medoids.

Compared with the *k*-means algorithm, the cluster centers obtained by the *k*-medoids algorithm necessarily correspond to real observed samples, i.e., actual network nodes in the power system. Since nodes within the same partition exhibit similar frequency variations, the selected medoid can effectively characterize the overall frequency behavior of the corresponding region. Based on these considerations, the *k*-medoids clustering algorithm is adopted in this paper, and the PMU-measured frequency of the medoid node is used as an approximate surrogate for the regional center-of-inertia (COI) frequency.

Based on Section 2.1 of this paper, a real-time partitioning method for frequency dynamic responses is constructed by using the DTW distance as the similarity metric in conjunction with the k-medoids algorithm. The specific implementation procedure is as follows:

1) Initial dynamic partitioning: The initial dynamic partitions are obtained using the Pearson-correlation-based spectral clustering method.

2) Cluster centers: According to (24), the distance sum between each node in a cluster and all other nodes within the same cluster is calculated. The node corresponding to the minimum sum is selected as the cluster center. The calculation is expressed as:

$$a = \min \sum_{\forall b \in A} L_{DTW}\left(f_m^a, f_n^b\right) \tag{24}$$

In the equation, Adenotes a specific region within the initial dynamic partition, $a$represents the cluster center of region A, and $b$refers to the remaining nodes in the region excluding a. The superscripts f_m^a and f_n^b correspond to the frequency trajectory curves of nodes $a$and b, respectively.

4 System Identification–Based Regional Inertia Estimation Process

After completing the dynamic partitioning and selecting the optimal frequency fitting nodes, a hierarchical representation framework is established, progressing from the overall system to regional equivalent frequency representation and further to regional representative nodal measurements. However, system inertia is not a directly measurable explicit parameter; rather, its dynamic characteristics are primarily reflected in the transient coupling relationship between active power disturbances and frequency responses. Therefore, based on the regional equivalent inertia observables and the corresponding power disturbance signals, a multi-method collaborative inertia estimation framework is constructed in this paper.

First, the N4SID subspace identification method is employed to develop a regional power–frequency dynamic model, from which inertia-related parameters are extracted through system poles and dynamic response characteristics. Second, a fast inertia estimation is obtained using the physical relationship between the initial rate of change of frequency (RoCoF) and the magnitude of the power disturbance. Third, an improved weighted least squares (WLS) method is introduced to perform statistical fitting over the entire frequency response process, thereby enhancing the stability and noise robustness of inertia parameter estimation. Finally, the inertia estimates obtained from multiple methods are fused to derive a regional inertia value with improved robustness and reliability. The multi-method fusion framework integrates transient physical information, system dynamic structural characteristics, and statistical optimization features, thereby mitigating the sensitivity of any single method to modeling assumptions or measurement noise.

4.1 Regional Inertia Identification Model Based on N4SID

In a regional power system, the frequency dynamic response is jointly determined by multiple synchronous generators, renewable energy sources, and loads within the region, and its equivalent dynamic characteristics typically exhibit low-order and strongly coupled behavior. As renewable energy penetration increases, the distribution of system inertia becomes time-varying and uncertain. Consequently, traditional parametric system identification methods based on a fixed model order and explicit noise modeling are limited in their applicability to complex regional systems.

To avoid prior assumptions regarding the model structure and order, this paper employs a subspace-based system identification method—Numerical algorithms for Subspace State Space System Identification (N4SID)—to model the regional power–frequency dynamic process. The N4SID method analyzes the geometric structure of input–output data in a high-dimensional space and directly extracts the system's state subspace from the data, thereby constructing a state-space model.

N4SID is a state-space model identification method based on subspace projection and singular value decomposition (SVD), which can simultaneously estimate the system order and model parameters from experimental data in the presence of noise. Given that the identification data are in discrete-time form, in each sliding time window, the N4SID discrete model identified at time $t$is converted to a continuous-time transfer function using the bilinear transformation method implemented via MATLAB's *d2c* function. The structure of the N4SID model and the corresponding bilinear transformation process are shown in (25).

$$\begin{cases} \boldsymbol{x}(k+1) = \boldsymbol{A}\boldsymbol{x}(k) + \boldsymbol{B}\boldsymbol{u}(k) + w(k) \\ \boldsymbol{y}(k) = \boldsymbol{C}\boldsymbol{x}(k) + \boldsymbol{D}\boldsymbol{u}(k) + v(k) \end{cases} \tag{25}$$

In the above formulation, $\boldsymbol{x}(k)$ denotes the state vector, $\boldsymbol{u}(k)$ the input vector, and **c**the output vector. Matrices **A**, **B**, **C**, and **D**are the system matrices to be identified. Variables $w(k)$ and $v(k)$ represent stochastic sequences corresponding to process noise and measurement noise, respectively.

Subspace identification techniques are capable of constructing state-space models directly from system operating data without the need to deliberately inject external disturbances, thereby offering strong practicality and flexibility. The core idea of the Numerical Subspace State Space System Identification (N4SID) method lies in obtaining the extended observability matrix $\boldsymbol{\Gamma}_k$ through oblique projection operations, the computational procedure of which is described as follows.

$$\Gamma_k = \left(Y_f \left/ \begin{bmatrix} U_P \\ Y_P \end{bmatrix} \right. \right) / U_f \tag{26}$$

Here, the symbol "/" denotes the oblique projection operation. To determine the order of the identified system model, singular value decomposition (SVD) is performed on the obtained matrix $\boldsymbol{\Gamma}_k$. In general, the number of dominant singular values of $\boldsymbol{\Gamma}_k$ corresponds to the effective system order. The SVD of $\boldsymbol{\Gamma}_k$can be further expressed in the following form.

$$W_1 \Gamma_k W_2 = \begin{bmatrix} U_1 & U_2 \end{bmatrix} \begin{bmatrix} S_1 & 0 \\ 0 & S_2 \end{bmatrix} \begin{bmatrix} V_1^T \\ V_2^T \end{bmatrix} \approx U_1 S_1 V_1^T \tag{27}$$

where $\mathbf{W}_1$ and $\mathbf{W}_2$ are identity weighting matrices. As shown in (27), since the dominant dynamic behavior of the system is primarily determined by the leading singular values, the components associated with smaller singular values can be neglected. Accordingly, model order reduction is achieved by truncating the singular value matrix $\mathbf{S}$. Subsequently, the state-space system matrices $\mathbf{A}$, $\mathbf{B}$, $\mathbf{C}$, and $\mathbf{D}$can be obtained by solving the corresponding sets of linear equations.

Since practical power systems usually comprise multi-layered and strongly coupled control structures, their intrinsic system order is typically high. In the identification process, a low-order equivalent model is therefore adopted in this paper. Although the identified model order is lower than that of the actual system, its dynamic characteristics are sufficient to capture the dominant inertia-related frequency response behavior. By predefining a model order search interval $[n_{\min}, n_{\max}]$, the N4SID method is able to automatically determine the optimal model order. Based on engineering experience and to ensure adequate accuracy in inertia parameter estimation, the parameters are set to $n_{\min} = 1$and $n_{\max} = 10$.

4.2 Multi-Method Fusion–Based Regional Inertia Estimation Strategy

In addition to the N4SID-based dynamic modeling approach, this paper further incorporates the RoCoF method and an improved weighted least squares (WLS) method as complementary techniques for regional inertia estimation. The RoCoF method exploits the direct physical relationship between the initial rate of change of frequency following a disturbance and system inertia, thereby enabling rapid characterization of the system's initial inertial response. In contrast, the improved WLS method performs statistical fitting over the entire frequency response trajectory, enhancing the stability and noise immunity of the inertia parameter estimation process.

The aforementioned methods emphasize different characteristic stages of the frequency dynamic response. The N4SID approach exploits full time-domain dynamic information for system modeling; the RoCoF method is more suitable for rapid physical estimation during the initial disturbance stage; and the improved weighted least squares (WLS) method performs noise-resistant statistical optimization. The organic integration of these three inertia estimation methods helps compensate for the limitations inherent in any single approach. Considering that different methods may yield outlier estimates under specific operating conditions, the proposed framework first performs dynamic partitioning based on real-time frequency trajectory correlations and constructs regional representative frequencies. Using the regional nodal frequency measurements and the active power of interconnecting tie-lines as input data, regional inertia is then estimated separately via the N4SID model, the RoCoF method, and the improved WLS method.

Subsequently, the multiple estimation results are adaptively weighted according to their confidence levels, and the fused output is taken as the final online assessment of regional inertia. This comprehensive estimation strategy maintains strong stability and adaptability under various disturbance types and operating conditions, thereby providing reliable support for real-time monitoring and analysis of regional inertia levels.

After completing the model identification process, the validity of the obtained model is verified. The estimation error is adopted as the evaluation metric, and the consistency between the predicted output $\hat{y}(t)$ and the actual measured output $y(t)$.is assessed by comparing the two signals to quantify the degree of agreement between model prediction and real measurement.

5 Case Study and Simulation

5.1 Experimental Simulation System Setup

This paper conducts simulation studies on the IEEE 39-bus system using MATLAB, and the system topology is shown in Fig. 6. The nominal system frequency is set to 60 Hz. According to PMU deployment principles, phasor measurement units are installed on high-voltage transmission lines and substations. For the equivalent IEEE 39-bus system, PMUs are deployed at all buses except the generator terminal buses.

The applied disturbance consists of small active power fluctuations in the load, with magnitudes constrained within the governor deadband to ensure that the system frequency deviation does not reach the governor activation threshold. Under this operating condition, the dynamic response of the regional frequency can be characterized by (5). The rated capacities and inertia constants of each generating unit are listed in Table 1, and the unified system base capacity is set to 1000 MVA.

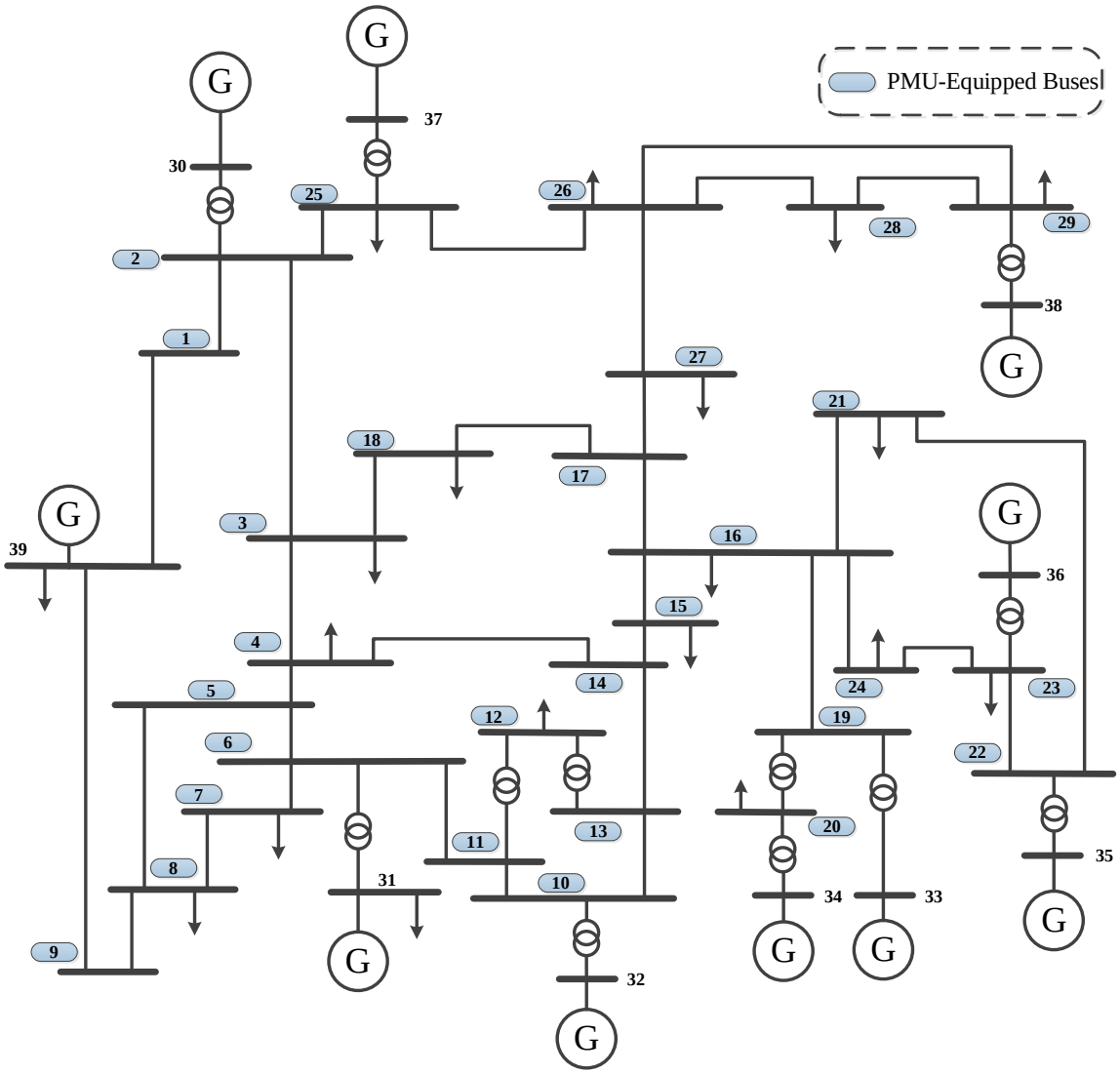

Figure 6: Topology of IEEE 39 system

Table 1: Parameters of Each Generator in the System

Generator Model Number	Rated Capacity/MVA	Inertia constant/s
G01	1000	5.00
G02	1000	4.48
G03	800	3.24
G04	800	3.58
G05	600	4.33
G06	800	3.54
G07	700	2.63
G08	700	3.77
G09	1000	3.45
G10	1000	4.20

5.2 System Frequency Dynamic Partitioning and Representative Node Selection Results Analysis

5.2.1 Validation of Dynamic Partitioning and Representative Node Selection Under Large-Disturbance Scenarios

At t = 5 s, a 400 MW active power disturbance is applied to the load connected to Bus 4 and maintained for 2 s before being removed, in order to simulate a severe load disturbance event. Figure 7 illustrates the frequency response curves of all PMU-equipped buses in the system over the time interval t = 5~6 s. As observed from the figure, following the disturbance, the nodal frequency responses exhibit noticeable spatial differences in terms of amplitude and recovery characteristics.

However, strong consistency is maintained in the response initiation instant and overall evolutionary trend, reflecting the regional correlation characteristics of system frequency dynamics. These observations provide a foundation for subsequent region partitioning based on frequency dynamic responses and for regional equivalent inertia assessment, while also offering a basis for comprehensive analysis of the total system inertia.

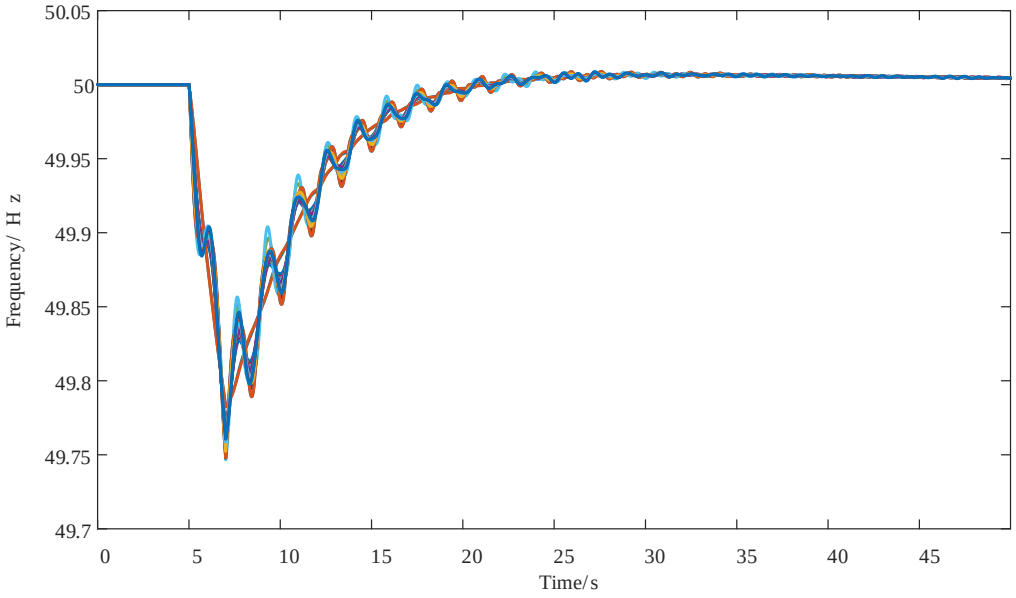

Figure 7: Generator Frequency Response Curve

As shown in Figure 7, the selected post-disturbance data window is used for real-time frequency dynamic partitioning analysis. Based on the frequency response trajectories of all nodes within this time window, the Pearson correlation coefficients between each pair of nodes are first calculated to quantify the consistency of their frequency variation trends. By characterizing the synchronicity and similarity of nodal frequency evolutions within the given window, a similarity matrix is constructed to reflect the dynamic behavioral characteristics of nodal frequency responses.

On this basis, a spectral clustering method is introduced to systematically partition the nodal frequency trajectories, thereby achieving frequency dynamic region identification. The partitioning results are shown in Fig. 9, where the system is divided into four regions: Region 1 includes generators G08 and G10; Region 2 consists of generators G04, G05, G06 and G07; Region 3 is formed independently by generator G01; and the remaining generator is assigned to Region 4.The quantitative evaluation results of each region are summarized in Table 2. The results indicate that the mean intra-regional correlation coefficients of all four regions exceed 0.93, and the consistency assessments reach the “excellent” level, demonstrating a high degree of synchronicity in the bus frequency dynamic responses within each region. These findings confirm that the proposed partitioning method based on frequency dynamic characteristics effectively captures the dynamic coupling relationships following system disturbances, and that the obtained regionalization results exhibit strong rationality and validity.

Table 2: Partition Evaluation Results

Region Indexing	Mean Intra-Regional Correlation Coefficient	Median Intraclass Correlation Coefficient	Consistency Evaluation Metrics
Zone 1	93.836%	98.567%	Excellent
Zone 2	99.704%	99.802%	Excellent
Zone 3	99.993%	99.996%	Excellent
Zone 4	99.999%	99.999%	Excellent

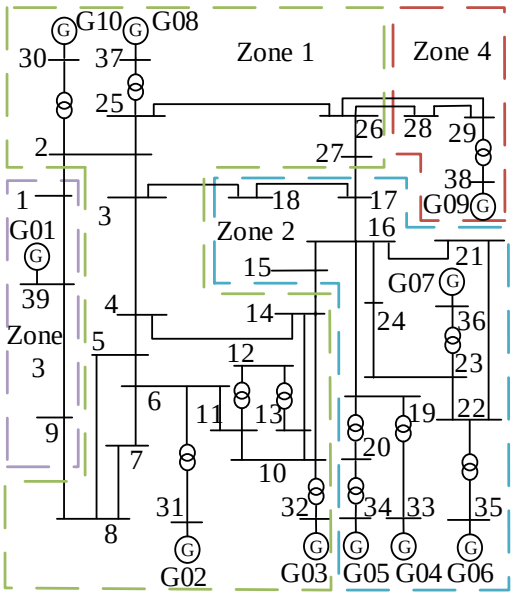

Figure 8: Regioning results

According to the above partitioning results, the frequency curves referenced in Figure 8 are reorganized accordingly. The nodal frequency response curves corresponding to Regions 1–4

are shown in Figure 9, respectively. It can be observed that, within the same region, the frequency response curves of different nodes exhibit similar magnitudes and comparable waveform characteristics, whereas the curves across different regions show pronounced discrepancies.

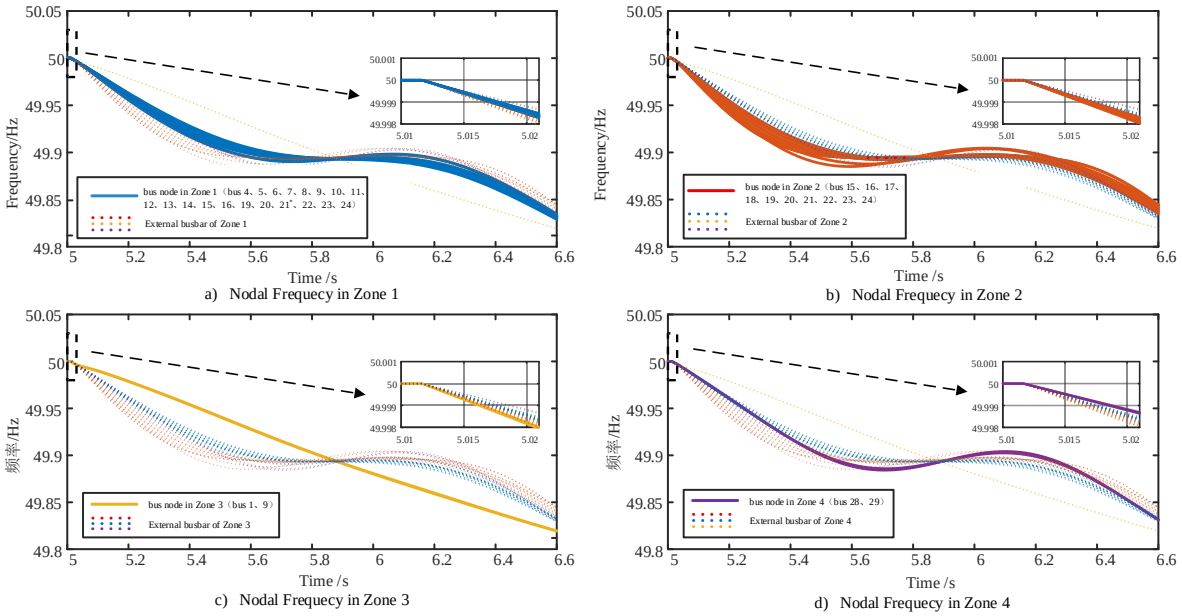

Figure 9: Comparative Plot of Frequency Responses Across Regions

To enhance the accuracy and stability of subsequent regional inertia estimation, a regional representative node selection mechanism is further introduced after completing the dynamic partitioning. Conventional approaches typically adopt the regional center-of-inertia (COI) frequency as the equivalent regional frequency measurement, which is usually constructed as a capacity-weighted average to form a virtual frequency signal. However, this method has limited capability in capturing the spatial heterogeneity of frequency dynamic responses within a region. Under high penetration of renewable energy sources, its effectiveness in representing equivalent regional inertia is further weakened. To address this issue, based on the dynamic partitioning results, this paper proposes a regional representative node selection strategy. The dynamic similarity among nodal frequency trajectories within each region is quantified using the Dynamic Time Warping (DTW) distance. Subsequently, the K-medoids algorithm is employed to select, from the set of actual physical nodes, the observation point whose frequency trajectory is closest to the regional central response trajectory. This selected node is then used to construct a physically interpretable regional equivalent frequency measurement.

Figure 10 presents the heat maps of the DTW distance matrices constructed from the nodal frequency trajectories within each dynamic region, along with the average edit distance of nodes in each region. In the heat maps, the color intensity reflects the degree of dynamic similarity between nodal frequency responses, with darker colors indicating higher similarity between the corresponding pair of nodes. On this basis, the K-medoids algorithm is applied to perform representative analysis within each region, selecting a regional representative node from the set of actual physical nodes to serve as the equivalent frequency measurement point. As shown in Figure 10, the representative frequency measurement nodes for Zone 1 through 4 are Bus 27, Bus 16, Bus 1, and Bus 28, respectively.

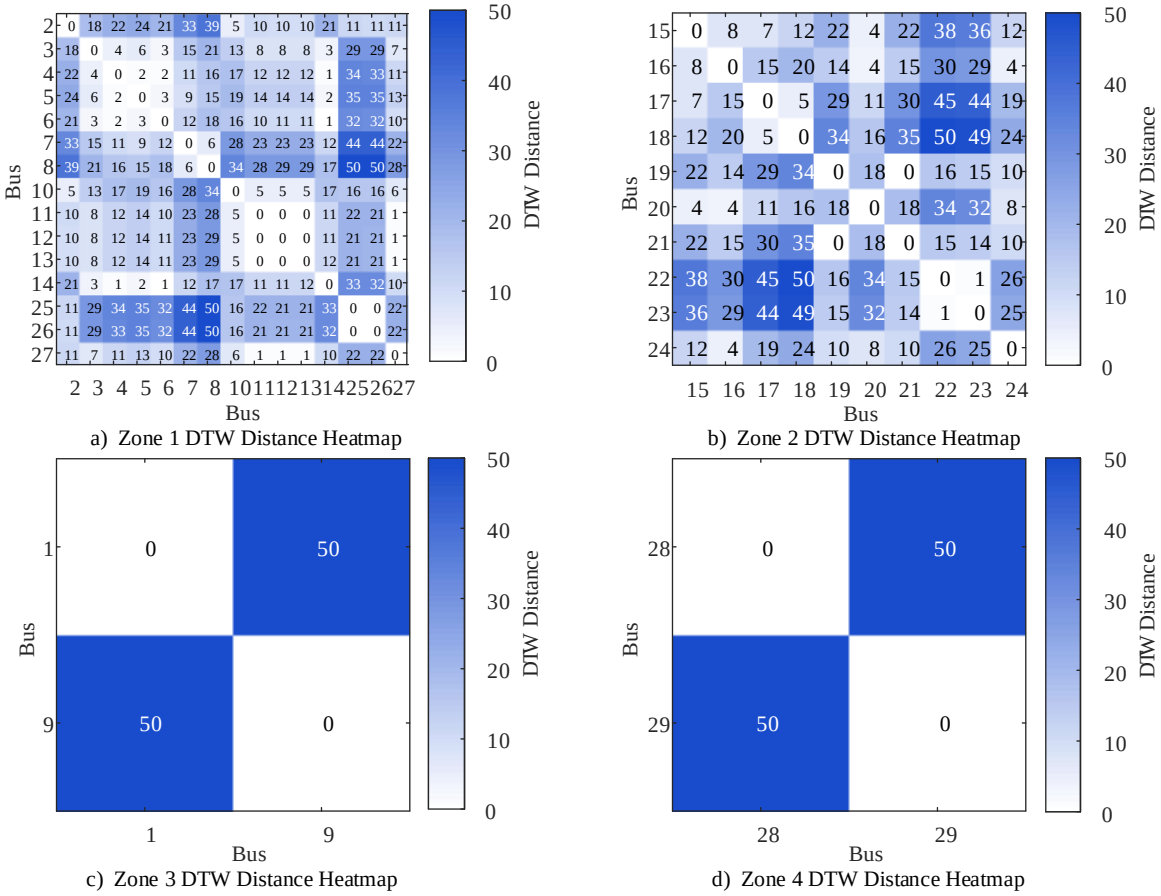

Figure 10: DTW Heat Maps of Each Region and Average Edit Distance of Nodes

To evaluate the effectiveness of the above node selection results, three key performance indices are adopted:

1) Coefficient of determination (R^2), used to quantify the explanatory capability of the selected node with respect to the regional average frequency trajectory; 2)Representativeness error, measured based on the DTW distance, to assess the similarity between the selected node's trajectory and those of other nodes within the same region; 3) Mean correlation coefficient, used to verify the consistency of frequency variation trends between the selected node and the remaining nodes in the region. The node selection results are summarized in Table 3. The average R^2 value of the selected nodes reaches 0.9757, the mean representativeness error is as low as 0.2847, and the average correlation coefficient is as high as 0.9922. These results indicate that the selected nodes effectively capture the frequency dynamic characteristics of their respective regions while simultaneously ensuring strong explanatory power and high trend consistency.

Table 3: Representative Node Selection Evaluation Results

Zone Index	Representative Node	R^2	Representativeness Error	Correlation Coefficient
Zone 1	Bus27	0.9112	0.2798	0.9711
Zone 2	Bus16	0.9923	0.3401	0.9978
Zone 3	Bus1	0.9995	0.3383	0.9999
Zone 4	Bus28	1.0000	0.1805	1.0000

5.2.2 Validation of Dynamic Partitioning and Representative Node Selection Under Small-Disturbance Scenarios

To verify the real-time performance of the proposed partitioning method and its adaptability to varying operating conditions, multiple disturbances are imposed on the IEEE 39-bus system to emulate practical grid frequency fluctuation scenarios. Specifically, small load disturbances of 5 MW are applied during t = 6~10 s and t = 20~24 s at load buses {4, 7, 8} and {21, 28, 29}, respectively.

Case studies are conducted using the data windows t = 6~10 s and t = 20~24 s as representative examples. First, from the qualitative observation in Fig. 13, it can be seen that the frequency responses of Bus 16 and Bus 17 exhibit almost no difference during t = 6~10 s after the disturbance, and thus can be classified into the same region. However, during t = 20~24 s, their frequency trajectories differ significantly and cannot be grouped into the same region. This indicates that the partitioning characteristics of the power system exhibit real-time variability.

The effectiveness of the proposed frequency-response-based partitioning method is illustrated in Figure. 11. Figures 11(a) and (b) present the partitioning results and the corresponding frequency response curves for the time window t = 6~10 s. During t = 6~10 s, significant differences in oscillatory characteristics are observed among the frequency curves, leading to the system being divided into two regions.

Similarly, Figure 12 presents the heat maps corresponding to the DTW distance matrices constructed for each zone. The K-medoids algorithm is employed to perform representative analysis within each zone, and the corresponding representative node is selected as the equivalent frequency measurement point. As shown in Fig. 15, during t = 6~10 s, the optimal frequency measurement nodes are Bus 16 for Zone 1, Bus 11 for Zone 2.

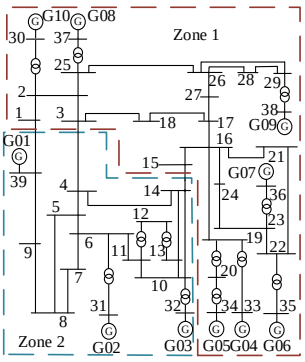

(a) Partitioning Results at t =6~10 s

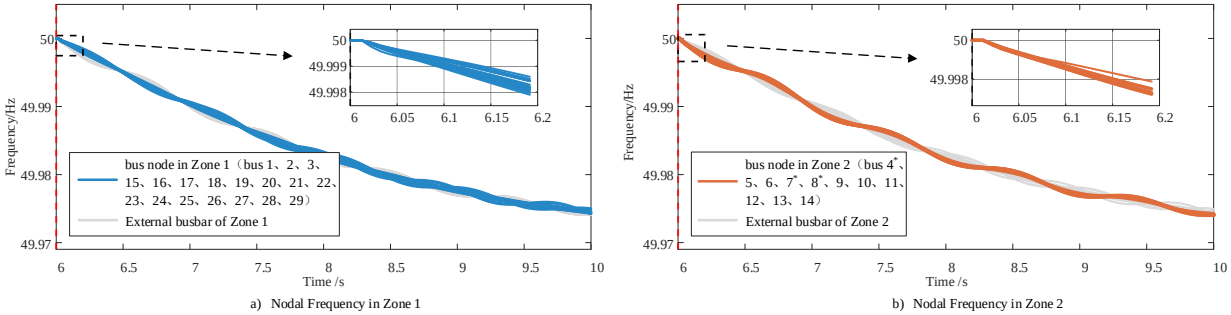

(b) Partitioning Results at t = 6~10 s

Figure 11: Partitioning Results and Comparative Frequency Responses of Each Zone

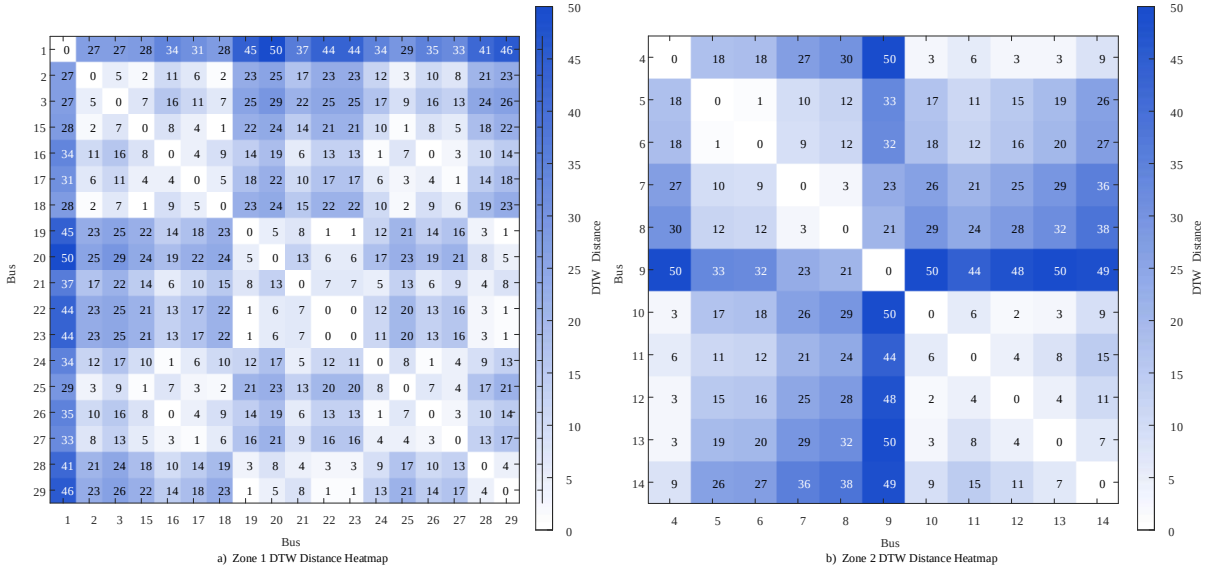

Figure 12: DTW Heat Maps of Each Region and Average Edit Distance of Nodes

While Figures 13(a) and (b) show the corresponding results for t = 20~24 s. As the disturbance location changes, the system partitioning results vary accordingly, and the cluster-center nodes are adjusted correspondingly. In contrast, during t = 20~24 s, the system is partitioned into three regions. As indicated in Figures 14, during t = 20~24 s, the optimal frequency measurement nodes are Bus 4 for Zone 1, Bus 17 for Zone 2, and Bus 26 for Zone 3.

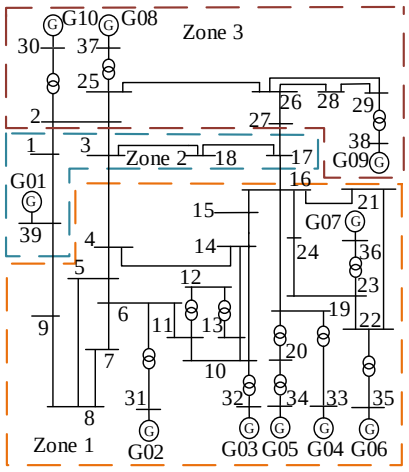

(a) Partitioning Results at t = 20~24 s

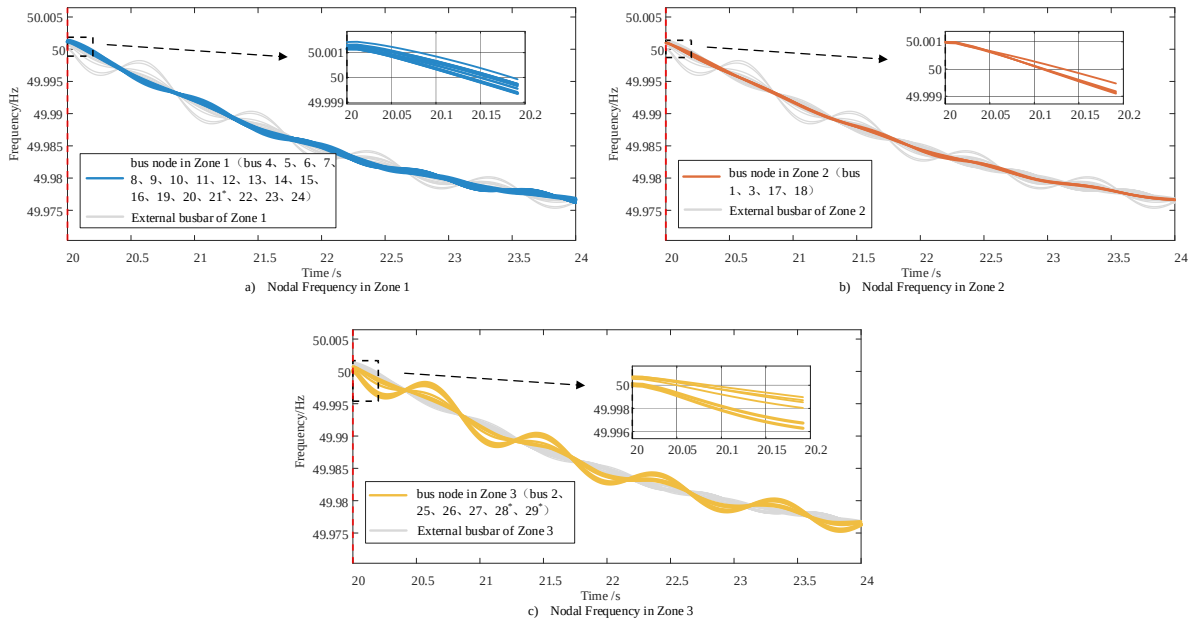

(b) Partitioning Results at t = 20~24 s

Figure 13: Partitioning Results and Comparative Frequency Responses of Each Zone

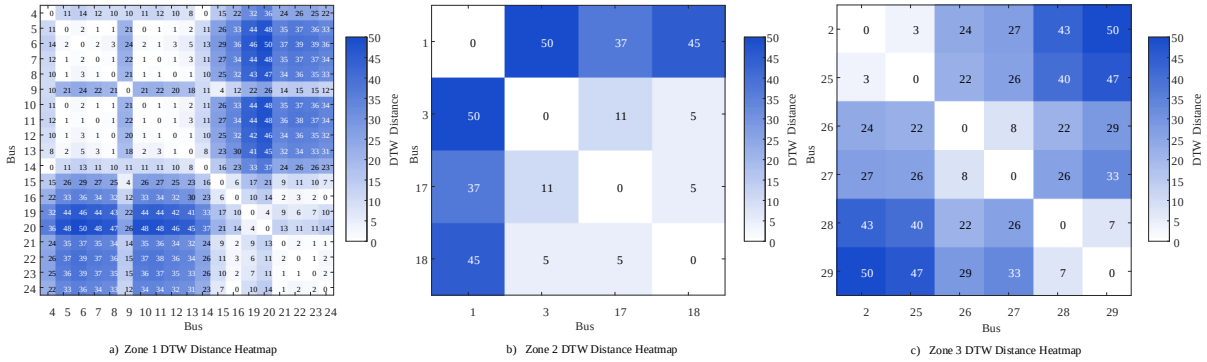

Figure 14: DTW Heat Maps of Each Region and Average Edit Distance of Nodes

5.3 Regional Inertia Estimation Results and Model Accuracy Validation

5.3.1 Analysis of Regional Inertia Estimation Results Under Different Disturbance Scenarios

In this section, inertia parameter identification is carried out under various disturbance scenarios described in Section 5.2. Compared with the conventional inertia estimation approach based on N4SID (Numerical Subspace State-Space System Identification), the improved algorithm proposed in this paper introduces multi-level optimizations in both modeling philosophy and implementation pathway.

In terms of data preprocessing and disturbance modeling, a two-stage moving average filtering is applied to the frequency deviation sequence. In addition, leading zeros and regional power-sharing coefficients are explicitly incorporated into the input signal, thereby effectively mitigating the influence of measurement noise and initial-condition uncertainty on state-space identification. This treatment substantially alleviates the high sensitivity of the original N4SID method to disturbance window selection and its tendency to become unstable under low signal-to-noise ratio conditions. At the system identification strategy level, instead of adopting a

single-model order or a single time window for N4SID estimation, this study introduces a parallel identification framework with multiple time windows and multiple model orders, combined with a goodness-of-fit screening mechanism. Furthermore, the RoCoF information is extracted from the linear slope of the step response during the initial disturbance stage, enabling the mapping from “black-box state parameters” to physically interpretable inertia constants. This strategy significantly enhances the stability and repeatability of the identification results. At the method integration level, the improved N4SID results are complementarily fused with those obtained from the classical RoCoF method and the weighted least squares (WLS) approach. Differentiated weights are assigned to each method according to the regional frequency dynamic characteristics, thereby constructing a robust multi-source inertia estimation framework.

In summary, compared with the original N4SID-based inertia estimation approach, the improved algorithm proposed in this paper not only significantly enhances the physical interpretability and numerical stability of inertia estimation, but also demonstrates stronger engineering adaptability and explainability at both regional and system levels. It therefore provides a reliable technical pathway for inertia assessment in power systems with high penetration of renewable energy sources. The corresponding inertia estimation results are summarized in Tables 4–6.

Table 4: Regional Inertia Estimation Results Under a 400 MW Large Disturbance

Zone Number	Actual Inertia /s	Identified Results /s	Error /%
Zone 1	14.135	14.307	1.22
Zone 2	12.020	11.800	1.83
Zone 3	5.000	5.137	2.74
Zone 4	3.450	3.514	1.87

Table 5: Regional Inertia Estimation Results Under a 5 MW Small-Disturbance Scenario(t = 6~10 s)

Zone Number	Actual Inertia /s	Identified Results /s	Error /%
Zone 1	26.575	26.307	-1.793
Zone 2	8.030	8.161	-2.066

Table 6: Regional Inertia Estimation Results Under a 5 MW Small-Disturbance Scenario(t = 20~24 s)

Zone Number	Actual Inertia /s	Identified Results /s	Error /%
Zone 1	16.485	16.236	1.51
Zone 2	8.030	7.940	1.12
Zone 3	10.080	9.887	1.91

5.3.2 Validation of Model Robustness and Accuracy Under Renewable Energy Integration Scenarios

To ensure the applicability of the proposed regional inertia estimation method under renewable energy integration conditions, the IEEE 39-bus system is adopted as the test platform. Generator G08 is replaced with an equivalent-capacity grid-following wind turbine generator equipped with an inertial control loop. Each wind turbine unit has a rated output power of 6.25 MW, a rated wind speed of 11.5 m/s, and an inertia time constant of 2.5 s. In addition, each wind turbine is configured with virtual inertia control and droop control loops, whose control parameters can be set online, demonstrating strong engineering practicability. By varying the virtual inertia and

droop control parameters of the wind turbines, the variation characteristics of regional inertia under different control strategies are analyzed, and the effectiveness of the proposed regional inertia identification model under renewable energy integration scenarios is validated.

Three different control parameter settings are considered. In the first case, no supplementary control is applied to the wind turbines, with the virtual inertia control gain and droop control gain set to zero (i.e., K_p=0 s , K_d=0). In the second case, the virtual inertia control parameter is set to K_p=-10 s and the droop control parameter to K_d=-20. In the third case, K_p=-10 s and K_d=-30. After integrating the renewable energy units into Zone 4, the equivalent regional inertia is identified using the proposed inertia estimation method. The variation patterns of equivalent inertia under different control strategies are compared, as shown in Figure 15. The simulation results indicate that, at the initial stage of the disturbance when system frequency begins to deviate, the virtual inertia control of the renewable energy units effectively enhances the equivalent inertia level of the region. After the disturbance is cleared and the frequency dynamics gradually stabilize, the virtual inertia support effect weakens progressively, leading to a reduction in the equivalent regional inertia, which eventually converges to the sum of the inertia constants of the synchronous generators within the region.

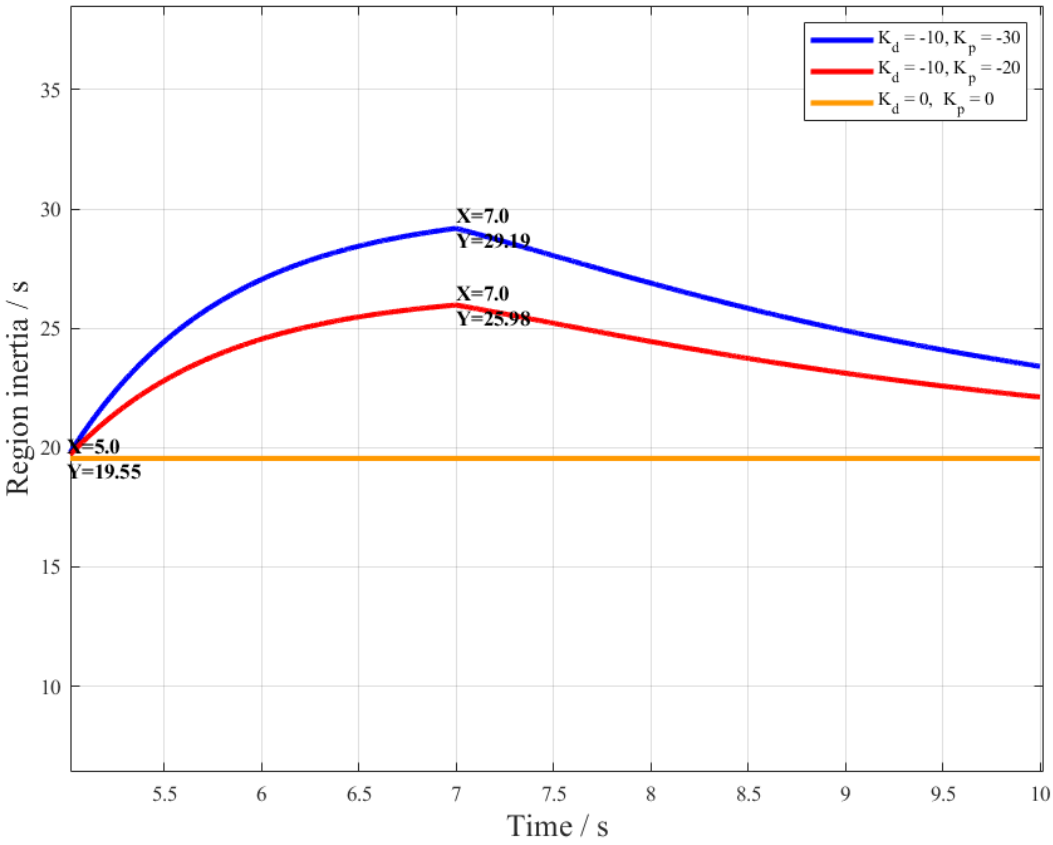

Figure 15: Comparison of Regional Equivalent Inertia Variations Under Different Virtual Inertia Control Strategies

The theoretical true values of regional inertia can be calculated according to Equation (4), providing reference inertia parameters for the three different control schemes. The identified inertia results are then compared with these theoretical values, and the error statistics are shown in Figure 16. It can be observed that, under all three control strategies, the inertia estimation errors remain consistently within approximately 2%, indicating that the proposed regional inertia estimation method maintains high accuracy and strong robustness even under renewable

energy integration conditions.

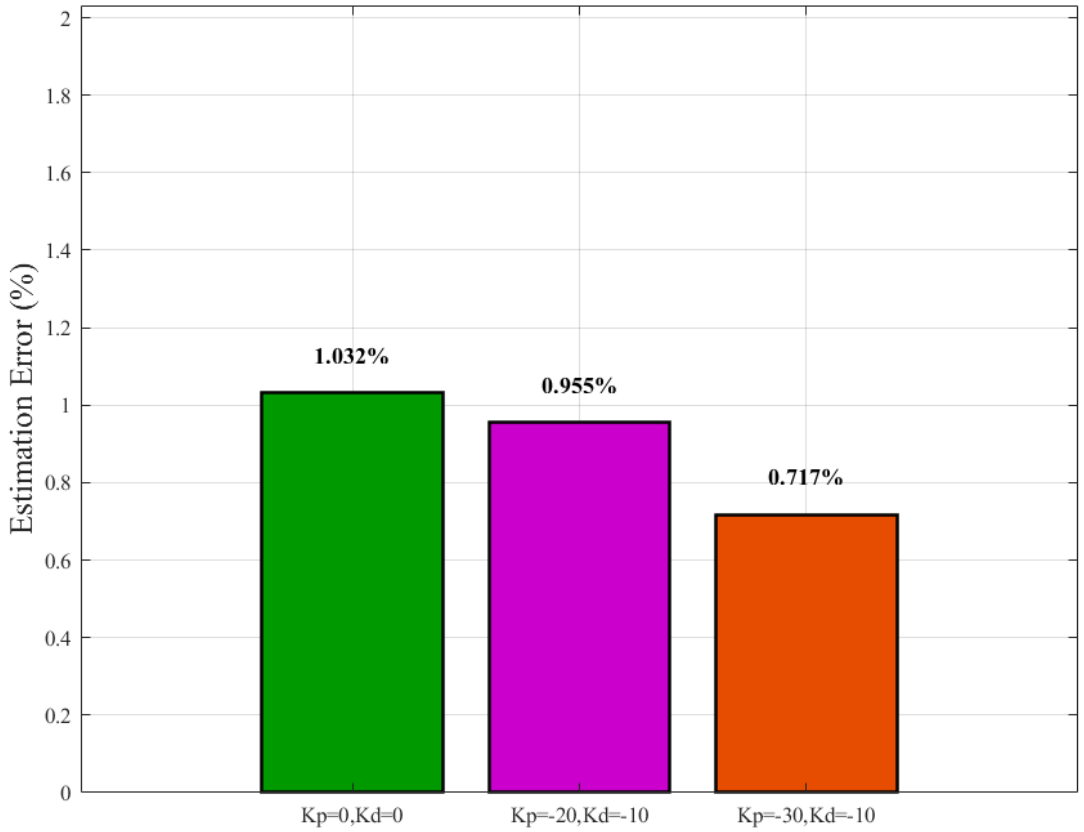

Figure 16: Comparison of Regional Inertia Accuracy Under Different Virtual Inertia Control Strategies

6 Conclusion

This paper proposes an online regional inertia assessment method based on frequency dynamic partitioning. The method exploits the correlation information among real-time frequency trajectories and employs a partitioning strategy that combines Pearson correlation coefficients with spectral clustering to achieve dynamic updates of system frequency regions within a sliding time window. By introducing DTW and K-medoids clustering, representative measurement nodes are selected within each region to construct equivalent regional frequency signals. Furthermore, the approach integrates N4SID state-space identification with multiple inertia estimation strategies through statistical fusion. The effectiveness of the proposed method is validated on the IEEE 39-bus system. The main conclusions are summarized as follows:

1) The partitioning of power system regions is closely related to the system operating point and the characteristics of disturbances. The Pearson–spectral clustering-based partitioning method proposed in this paper enables real-time updating of regional boundaries, fully accounting for the network topology and the dynamic frequency responses of system nodes.

2) Based on the above partitioning results, DTW and K-medoids algorithms are employed to dynamically identify the regional equivalent (center-of-inertia) frequency, providing a foundation for subsequent model parameter identification.

3) A multi-method inertia estimation model based on the improved N4SID is constructed. Compared with conventional inertia estimation approaches, this model achieves higher accuracy, reaching 98% or above.

Building on this, future research will focus on scenarios with high renewable energy integration, aiming to develop a real-time dynamic partition adjustment system that continuously tracks internal system frequency fluctuations and formulates optimal operational strategies.

References

[1] Z. Zhang, N. Zhang, E. Du, et al., Review of Frequency Security Issues and Countermeasures in Dual-High Power Systems, in Proceedings of the Chinese Society for Electrical Engineering, vol. 42, no. 1, pp. 1-25, Jan. 2022.

[2] Tan B, Zhao J, Netto M, et al. Power system inertia estimation: Review of methods and the impacts of converter-interfaced generations[J]. International Journal of Electrical Power & Energy Systems, 2022, 134:107362.

[3] Jianing Luo, Hangxin Li, Shengwei Wang, A quantitative reliability assessment and risk quantification method for microgrids considering supply and demand uncertainties, Applied Energy, Volume 328, 2022,120130.

[4] P. Du and W. Li, "Frequency Response Impact of Integration of HVDC Into a Low-Inertia AC Power Grid," in IEEE Transactions on Power Systems, vol. 36, no. 1, pp. 613-622, Jan. 2021.

[5] Kerdphol T , Watanabe M , Nishikawa R ,et al.Inertia Estimation of the 60 Hz Japanese Power System From Synchrophasor Measurements[J].Power Systems, IEEE Trans. on (T-PWRS), 2023, 38(1):14.

[6] Makolo P , Zamora R , Lie T T .The role of inertia for grid flexibility under high penetration of variable renewables - A review of challenges and solutions[J].Renewable and Sustainable Energy Reviews, 2021, 147(5):111223.

[7] Tan B , Zhao J , Terzija V ,et al.Decentralized data-driven estimation of generator rotor speed and inertia constant based on adaptive unscented Kalman filter[J].International Journal of Electrical Power & Energy Systems, 2022, 137:107853

[8] XU Bo, ZHANG Linwei, YU Xiangdong, et al. An improved method of power system inertia online estimation based on system identification[J]. Power System Protection and Control, 2021, 49(18): 62-69.

[9] R. J. Best, P. V. Brogan and D. J. Morrow, "Power System Inertia Estimation Using HVDC Power Perturbations," in IEEE Transactions on Power Systems, vol. 36, no. 3, pp. 1890-1899, May 2021.

[10] C. Phurailatpam, Z. H. Rather, B. Bahrani and S. Doolla, "Measurement-Based Estimation of Inertia in AC Microgrids," in IEEE Transactions on Sustainable Energy, vol. 11, no. 3, pp. 1975-1984, July 2020.

[11] P. Wall and V. Terzija, "Simultaneous Estimation of the Time of Disturbance and Inertia in Power Systems," in IEEE Transactions on Power Delivery, vol. 29, no. 4, pp. 2018-2031, Aug. 2014.

[12] Y. Wang, H. Silva-Saravia and H. Pulgar-Painemal, "Estimating inertia distribution to enhance power system dynamics," 2017 North American Power Symposium (NAPS), Morgantown, WV, USA, 2017, pp. 1-6.

[13] ASHTON P M, SAUNDERS C S, TAYLOR G A, et al. Inertia estimation of the GB power system using synchrophasor measurements[J]. IEEE Transactions on Power Systems, 2014, 30(2): 701-709.

[14] K. Tuttelberg, J. Kilter, D. Wilson and K. Uhlen, "Estimation of Power System Inertia From Ambient Wide Area Measurements," in IEEE Transactions on Power Systems, vol. 33, no. 6, pp. 7249-7257, Nov. 2018.

[15] J. Fradley, R. Preece and M. Barnes, "The Influence of Network Factors on Frequency Stability," in IEEE Transactions on Power Systems, vol. 35, no. 4, pp. 2826-2834, July 2020.

[16] Pulgar-Painemal H , Wang Y , Silva-Saravia H .On inertia distribution, inter-area oscillations and location of electronically-interfaced resources[J].IEEE Transactions on Power Systems, 2017:1-1.

[17] T. Zhou, J. Wu, Y. Qiao, M. Dai, W. Gu and Z. Chen, "Power System Region Partition Method with High-Penetration of Renewable Energy Considering Frequency Temporal-Spatial Distribution Characteristics," 2025 4th Conference on Fully Actuated System Theory and Applications (FASTA), Nanjing, China, 2025, pp. 01-07.

[18] H. Gao, H. Xin, G. Hu, H. Yuan, L. Huang and P. Ju, "Common-Mode Frequency of Power Systems Affected by Voltage Dynamics," in IEEE Transactions on Power Delivery, vol. 39, no. 6, pp. 3279-3291, Dec. 2024.

[19] P. M. Ashton, C. S. Saunders, G. A. Taylor, A. M. Carter and M. E. Bradley, "Inertia Estimation of the GB Power System Using Synchrophasor Measurements," in IEEE Transactions on Power Systems, vol. 30, no. 2, pp. 701-709, March 2015.

[20] XU Bo,YANG Yixin,YU Wanqiang,et al. Power system iner-tia identification based on a state space model and a PEM iterative algorithm[J]. Power System Protection and Control.2022,50(18):123-130.

[21] JIA Jiaoxin,SHEN Zhongyu,QIN Benshuang,et al. Review on inertia response matching problem of hybrid power systems with grid-forming and grid-following power electronic devices[J]. Electric Power Automation Equipment,2024,44(6):77-89.

[22] J. Liu, C. Wang, T. Bi and G. Xu, "Online Estimation of POI-Level Aggregated Inertia Considering Frequency Spatial Correlation," in IEEE Transactions on Power Systems, vol. 38, no. 4, pp. 3232-3244, July 2023.

[23] Makolo P, Oladeji I, Zamora R, et al. Data-driven inertia estimation based on frequency gradient for power systems with high penetration of renewable energy sources[J]. Electric Power Systems Research, 2021, 195: 107171.

[24] Liu K Z, Tan H P, Yang C H, et al. Regional inertia estimation method for power systems considering system partitioning and node frequency dynamic response[J]. Electric Power

Automation Equipment, 2025, 45(05): 200-208.